LA-UR- 02-2853

Title: Corrosion Measurements on APT Prototypic Materials in the LANSCE High-Power Proton Beam and Applicability to Other Systems

Author(s): Lillard, R.S., Chandler, G.T.[a], Ferguson, P. D.[b], Gac, F.D., James, M.R., Maloy, S.A., Paciotti, M.A., Waters, L.S., and Willcutt, G. J.
Los Alamos National Laboratory
[a] Westinghouse Savannah River Company
[b] Oak Ridge National Laboratory

Submitted to: Third International Workshop on the Utilization and Reliability of High Power Proton Accelerators, Santa Fe NM, May 12-16, 2002.

Los Alamos
NATIONAL LABORATORY

Corrosion Measurements on APT Prototypic Materials in the LANSCE High-Power Proton Beam and Applicability to Other Systems

Lillard, R.S., Chandler, G.T.[a], Ferguson, P. D.[b], Gac, F.D., James, M.R., Maloy, S.A., Paciotti, M.A., Waters, L.S., and Willcutt, G. J.
Los Alamos National Laboratory
[a] Westinghouse Savannah River Company
[b] Oak Ridge National Laboratory

Abstract
The corrosion rates of several "corrosion resistant" materials behave in a similar manner even under the intense radiation of the LANSCE high-power beam. A second observation was made, showing that the corrosion rates saturated under high instantaneous radiation intensity in corrosion experiments conducted for the Accelerator Production of Tritium (APT) program. The LANSCE H^+ beam is not prototypic of the proposed APT production plant in several respects. The instantaneous proton flux in the APT production plant beam is about 10 times that of the LANSCE beam. The small transverse APT beam spot is rastered to spread the power density over the area of the target, and as the beam rasters, it creates a pulsed character to the beam at a specific location. In order to develop correlations that would enable extrapolation of the corrosion data to the proposed APT production plant, the experimental program included measurements over a range of average beam currents, measurements at high and low instantaneous beam current, and measurements at various combinations of pulse width and repetition rate. The correlations that were developed are based on an approximately linear dependence of corrosion rate on average beam current (average radiation intensity) and the saturation effect observed at high instantaneous radiation intensity. For a given transverse beam profile and for the same average beam current, the correlations predict the highest corrosion rate in a dc beam and the lowest corrosion rate in the lowest duty cycle beams. In the case of the APT extrapolation, the predicted corrosion rates were a factor of 5 lower than for a dc beam depositing the same average power density. The measured corrosion rates and the formulated extrapolations are applicable to water-cooled targets and components in proton beams.

Introduction
Corrosion experiments for the Accelerator Production of Tritium (APT) program were conducted with the high-power LANSCE H^+ beam which is not prototypic of the proposed APT production plant in several respects. The instantaneous proton flux in the APT production plant beam is about 10 times that of the LANSCE high-power beam. The small transverse APT beam spot is rastered to spread the power density over the area of the target. As the beam rasters, it creates a pulsed character to the beam at a specific location, similar to the LANSCE beam. Thus, the corrosion program included measurements over a range of average currents, measurements at high and low instantaneous power density, and measurements at various combinations of pulse width and repetition rate in order to develop correlations that would enable extrapolation of corrosion data to the conditions in the production plant.

Corrosion data

Corrosion rates of Alloy 718, 316L stainless steel, and aluminum Alloy 6061-T6 located in the intense LANSCE H^+ beam have been measured as part of the APT program [1]. Two other corrosion resistant materials, Alloys 625 and C276, were also included in the irradiation as alternate materials. Figure 1 shows the layout of the corrosion probes with respect to the proton beam flux profile which is approximately Gaussian in both transverse dimensions with σ's of 1.85 cm. Surprisingly, both of the candidate materials and the alternates located in the proximity of the 340 μA beam showed similar corrosion behavior as seen in Fig. 2. The 316L SS probe within Tube 40 is out of the proton beam and has a lower corrosion rate than the others shown in Fig. 2.

A general feature of the data and is that corrosion rates increase with average proton beam current (Figs. 3 & 4). Specifically, corrosion rates increase with average beam current as a power law, and the exponent is not far from 1.0 for all the materials studied [1]. These data are referred to in the text as the "average beam current series". Beam parameters are given in Table 1.

Table 1 Proton beam parameters for corrosion data for Figs. 3 & 4, the average beam current series. Duty cycle is Repetition Rate times Gate Length.

Average Current (mA)	Peak Current (mA)	Repetition Rate (Hz)	Gate Length (μs)	Duty Cycle
0.010	16	3	200	0.0006
0.036	16	10	200	0.002
0.10	16	10	625	0.00625
0.34	16	36	625	0.0225

It was noticed early, from the preliminary online results, that the corrosion rates did not fall off transversely to the beam centerline as steeply as did the current density of the proton beam. Referring to Fig. 5, it is seen that proton beam power falls faster than do the corrosion rates. In addition, Probes 35 and 38 of the same material (316L SS) located at the same transverse distances from the beam centerline exhibit significantly different corrosion rates.

The Influence of Duty Cycle

A second set of measurements, termed the "duty cycle series", explored a range of beam delivery parameters (instantaneous proton beam current[1], proton pulse width, and repetition rate). The purpose of this series was to extrapolate the corrosion observations to conditions in the production plant. The duty cycle experiment employed two peak currents, the maximum available 16 mA and another ten times smaller (1.6 mA). The average current was held constant by increasing the repetition rate for the 1.6 mA run by a factor of 10. The experiment found approximately a factor of two lower corrosion rate for the 16 mA instantaneous current than for the 1.6 mA case, suggesting a saturation effect; for example, additional protons above a threshold flux do not add to the corrosion kinetics. Corrosion efficiency is introduced in Ref. 2 as part of the discussion of corrosion measurements in pulsed beams.

[1] There is underlying micro pulse structure comprised of sub-nanosecond width pulses at 5 nanosecond spacing, but this time structure is not considered in this analysis. Peak current and instantaneous current are therefore used interchangeable in the text.

Table 2 Corrosion rates for Alloy 718 (Tube 33) as a function of average beam current, peak current, gate length, and repetition rate. The Electrochemical Impedance Spectroscopy (EIS) technique averages the corrosion rate over the surface of the probe. Throughout the text, Tube number and Probe number are used interchangeably.

Peak current (mA)	Average current (mA)	Beam pulse width (μs)	Repetion rate (Hz)	Corrosion rate (μm/y)
16	0.010	600	1	0.17
16	0.010	200	3	0.17
16	0.033	200	11	0.23
1.6	0.010	625	10	0.26
1.6	0.010	200	31	0.35
1.6	0.035	605	35	0.38
1.5	0.030	220	100	0.55

Data presented in Table 2 explored pulse width, repetition rate, and peak current. Consider subsets of Table 2 where average beam current and pulse width are constant. It is seen that high instantaneous beam current has a lower corrosion rate for the same average beam current. See Ref. 2 for specific operating conditions for these measurements. According to these data, a corrosion efficiency (taken as1.0 at low instantaneous radiation intensity) drops to approximately 0.5 at the highest available instantaneous radiation intensity.

It might be anticipated that the corrosion rate during the beam pulse is greater than the rate between beam pulses. And, in fact, we show evidence for transient effects in corrosion: The 1.6 mA peak current corrosion rates measured at 0.010 mA average are very interesting. Data were taken with the same corrosion probe at the same peak beam current and the same average beam current, where only the pulse length (and repetition rate) changed. A saturation-like effect, similar to the high instantaneous beam current saturation, is seen. Evidently, the saturation effect extends in time. The smaller corrosion rate was observed for the longer pulse length, constituting the discovery of a time constant in the process. The time constant can be thought of as a persistence, i.e., the radiation-induced effect must persist for a length of time in order to explain the observation. For example, corrosion near the tail end of the 600 μs beam pulse is apparently suppressed by the presence of beam about 600 μs earlier in the same beam pulse. Corrosion transient modeling described in Ref. 2, replicates the trends in the Table 2 data by including a relaxation time for the corrosion rate after the beam pulse.[2] The fact that the identical effect is not seen at 16 mA peak beam current could be attributed to an already saturating corrosion effect due to the high instantaneous beam current.

[2] It is not demonstrated conclusively that the corrosion rate itself undergoes a transient, but some physical change leading to corrosion does have a transient behavior.

Empirical correlations

In order to extrapolate to the APT plant conditions or other situations, interpretations of corrosion incorporate the observation that corrosion rates increase with average beam current as a power law under conditions where the instantaneous beam current is constant. An expression is constructed that seeks to find a common explanation for the influence of the duty cycle described above, the transverse fall off of corrosion rate (Fig. 5), and saturation at high beam intensity (i.e., corrosion efficiency). Qualitatively, the probes in the center see more intense beam than the off-axis probes, the corrosion rate for them is suppressed by the corrosion efficiency, giving rise to a broader transverse distribution (Fig. 5).

To find such an expression it was first necessary to calculate the particle distributions and their respective energies. Complete three dimensional geometry of the corrosion insert and the proton beam parameters were input to the MCNPX code, and detailed computations of radiation intensity were computed for each corrosion probe.

Since we do not know which particle type(s): proton, photon, neutron, is (are) primarily responsibility for the radiation-enhanced corrosion observed in these experiments, we are not sure which of the MCNPX predictions should be used to correlate with the measured corrosion rates. The differing spatial distributions of the particles might form a basis for deciding which are involved in corrosion. In fact, neutron and/or photon power densities (Table 5) correlate with trends in corrosion rate (Fig. 2). However, there are not a sufficient number of corrosion measurements to evaluate different weightings of each particle type in determining corrosion rate. Therefore, the simplest descriptor of radiation intensity, the total energy deposited for all particles combined, is the one exploited in this paper. (See Discussion section regarding Probes 35 and 38.)

Table 5 - Results from radiation transport calculations for tubes containing 316L SS samples. Flux was averaged over the tube length and summed for all particle energies. The relative fluxes permit comparison between corrosion probes but not between particle types.

Probe #	Relative proton flux	Relative neutron flux	Relative photon flux
35	72.7	38.0	35.2
36	127	52.7	46.2
38	70.9	43.8	37.3
40	6.0	13.5	13.2

The corrosion rate is formulated as an average over the length of the probe of the local power density[3] times the efficiency e which is a function of the instantaneous power density:

$$CR = a\sum_{l} P^{0.95} e\left(P_i\right) \tag{1}$$

where CR is the average corrosion rate of the probe in μm/y, a is the conversion factor from power density to corrosion rate in μm/y per W/cm^3, P is the local time-averaged power density in W/cm^3, e is the corrosion efficiency and is a function of the instantaneous power density, and P_i is the instantaneous power density and is equal to:

$$P_i = \frac{P}{DutyFactor} \tag{2}$$

where the *duty factor* is equal to the pulse width in seconds multiplied by the repetition rate in Hz.(e.g., Table 1). This expression reproduces the overall characteristics of the experiments plotted in Fig. 3 (the beam current series). The experiments performed at different beam currents found that the corrosion rate for 316L SS increases nearly linearly with average beam current (the dependence is a power law with exponent 0.95) where instantaneous beam current was always constant [1]. Since the power density at any point in the probe is directly proportional to average beam current, the exponent 0.95 can be applied to P as given by Eq. 1.

Correlations between total power density and corrosion rate were made for the 316L SS data because these probes were located directly on the beam centerline as well as several cm from centerline, allowing the corrosion rates to be analyzed over a wide range of P. The set of corrosion measurements for 316L SS considered in this analysis were conducted at an average beam current of 340 μA, a pulse width of 625 μs, and a repetition rate of 36 Hz. A functional form for e was created and trial values assumed in order to complete the prediction of corrosion rate from Eq. 1. The predictions of Eq. 1 were then fitted to the measured corrosion rates for each 316L SS probe [1] by varying the parameters for e and the value of the conversion factor, a.

The 16 and 1.6 mA peak current data of Table 2 would be prime information for the proposed fit because the factor of 10 change in P_i would be valuable in fitting the dependence on P_i. But since Table 2 applies entirely to Alloy 718 Probe 33, the data cannot be included directly in the fitting procedure for 316L SS probes. Taking advantage of the similarity between the Alloy 718 and 316L under radiation, a *ratio* of Alloy 718 corrosion rates from Table 2 could be included. The 600 μs, 10 μA average-current data was selected, and the corrosion rate ratio between the two peak currents was included in the fit, that is, Eq. 1 was required to predict the experimental

[3] It must be considered whether temperature increase due to higher power density is responsible for the increasing corrosion rates. This possibility has been examined and it was concluded that the calculated probe surface temperatures cannot account for the large increase in corrosion rates seen in Fig. 3.

ratio. According to Eq. 1, when e is multiplied (weighted) by a P distribution such Probe 33 in Fig. 6, the corrosion rate is suppressed in the center of the probe. Figure 7 displays a typical fitted corrosion efficiency distribution over the length of Probe 33 for two peak currents.

A single-parameter function for e that fits the 316L SS data at 340 μA is an exponential with decay constant of *0.000063 per W/cm*^{3}, while the conversion a was found to be *0.114 m/y per W/cm*^{3}. Figure 8 shows e and the scale of the instantaneous power density with an arrow marking the maximum extent of the experimental data. The saturation effect leading to Fig. 8 suggests a continued drop in e, however, since there is little theoretical or experimental guidance, there is little merit in attempting to extrapolate a long way to the high instantaneous power. Alternately, other functions were examined that have excellent fitting behavior over the range of available data but extrapolate as a constant corrosion efficiency at high instantaneous power density. The expression

$$e = 0.2 + \frac{0.8}{1 + \left(P_i / 7846 \right)^{1.39}} \qquad (3)$$

was selected (Fig. 9) that tracks the exponential out to the limit of the experimental information and then places an arbitrary asymptotic limit of 0.2 on the corrosion efficiency. The extra fitting variables are for the convenience of having a definite formula for corrosion efficiency and do not detract from the ability of the exponential to fit e with one variable.

The measured corrosion rates for Probes 35 and 38 differ by 38% (Fig. 2), and these are averaged for the fit because the computed P for these are nearly identical as previously discussed. We note here that Table 5 does predict a difference between Probes 35 and 38 based on neutron or photon flux, although not as great as measured. (See Discussion.)

Another variation taken adds a constant corrosion rate to Eq. 1 and treats it as a fitting variable, resulting in greatly improved quality of fits. The preferred value for this constant corrosion rate is *0.73 mm/y*. Although not strongly motivated, this constant can be thought of as the corrosion rate at a location where the power density is zero, such as an out-of-beam region where water chemistry effects dominate.[3] [4]

Extrapolation to the APT Production Plant Beam Conditions

The instantaneous power density under APT production plant [5] conditions is determined from the beam raster that sweeps a spot beam uniformly over the APT target. Any location in the complex raster sees a repetitive pulse train of eleven 50 μs wide pulses spaced by 4.1 ms where the amplitude of the pulses varies as a Gaussian with a σ of 4.65 ms. As an approximate comparison, the maximum instantaneous power densities in the pulse train are 10 times higher than are present on the corrosion probes. Therefore, according to Fig. 9, the corrosion efficiency

is about 0.2 and rises to 1 when the rastered beam spot is far from the location in question. Eq. 1 now becomes a sum over the individual pulses in the train:

$$Corrosion\ \ Rate = 0.73 + 0.114 \sum_{pulses} P^{0.95} e\left(P_i\right) \qquad (4)$$

The corrosion data from the beam current series (Fig. 3) supports the premise that the corrosion rate is additive for pulsed beams, and the duty-cycle series supports the premise that corrosion rate is additive for different peak current beam pulses, once accounting is made of e.

Figure 10 summarizes the effect of the beam time-structure on local corrosion rate. With no time structure (dc beam) the local corrosion rate would follow the upper curve. The middle curve (LANSCE beam) shows the behavior of corrosion as the beam current is increased, ending up at a 0.34 mA and a time-averaged power density of 300 W/cm^3. The lower curve is the predicted corrosion rate for the APT rastered beam from Eq. 4 as the average power density is increased to maximum (at the design current of 100 mA). The corrosion rates at low power density all initially follow the dc beam case and then increase more slowly as the corrosion mechanism begins to saturate.

From Fig. 10, the APT rastered beam is predicted to produce a corrosion rate of 20 μm/y in the 316L SS cladding [5] of the tungsten target cylinders.

Predictions for corrosion probe examinations

The EIS method is ideally suited to determining the corrosion performance of the APT candidate materials: 1) It is a sensitive on-line method for measurement under specific controlled beam conditions and water chemistry parameters. 2) A number of materials can be examined under the identical conditions, enabling the correlations drawn in this report. 3) Aqueous corrosion is electrochemical in nature and so it is natural to utilize an electrochemical technique where the corrosion current determines directly the rate of loss of structural metal.

Nevertheless, post-irradiation examination of the corrosion probes was carried out in attempt to confirm the EIS measurements. Eqs. 3 & 4 predict the corrosion distribution over the lengths of the 316L SS probes (Fig. 11) during the measurement period of approximately 10 days. Predicted corrosion in the center of the probe is only 0.3 μm. Moreover, the probes accumulate corrosion over the entire period of irradiation which lasted 2 months, and during most of this time other APT experiments located upstream of the corrosion experiment heavily interacted the core of the proton beam, leaving the predicted corrosion distribution shown in Fig. 12. The sum of Figs. 11 & 12, is the predicted corrosion over the course of the entire irradiation and is a fairly flat distribution. Even small relative changes along the length were difficult to discern[4], and diametrical variations, measured in the hot cell, could not detect corrosion of the center of the probes with respect to the ends within a measurement uncertainty of 2.5 μm.

[4] Corrosion rates measured with EIS are the rate of loss of structural metal; in general, it is not determined whether corrosion will result in a build up of oxide scale or a decrease in thickness. Corrosion can increase a probe diameter due to oxide buildup or decrease it if the oxide sluffs off.

The 304L SS cover plates for the materials irradiation experiment [6] offer a more sensitive test since they saw a narrow proton beam profile for a longer period of time (6 months). Using Eqs. 3 & 4 and computed power densities, predictions for the corrosion that should occur over the length of the cover plates are presented in Fig. 13. However, measurements of the cover plates (Table 7) could not detect corrosion of the center of the plates with respect to the ends within a measurement uncertainty of 5 μm and thus present a discrepancy with Fig. 13.

Table 7 – 304L Cover Plate thickness measurements. The thickness measurement of envelope 4-5 was compromised by the presence of corrosion products on the inside of the plate due to water leaking inside the envelope.

304L Envelope designation	Thickness at End (mils)	Thickness at Center (mils)	Thickness at End (mils)
control	9.5	9.6	9.5
1-5	9.8	9.8	9.7
2-5	9.5	9.6	9.4
4-5	9.4	9.2	9.1

Based on the data and analysis presented, there is good confidence that the corrosion distribution should be peaked in the center of the cover plates. Looking at Fig. 5, corrosion is peaked on the probe that is in the center of the proton beam. Thus, there is every reason to believe that the 304L cover plate corrosion should peak in the center as well[5].

Some of the possibilities that could reconcile the predictions of Fig. 13 and the measurements of Table 7 are the following:

1. The cover plates were cooled with a different water system than that used for the corrosion experiment, with largely unknown characteristics.
2. The cover plates formed an envelope for the materials radiation effects samples and were welded around the perimeter of the envelope, forming a water-tight seal in most instances. Evidence of corrosion was observed on the insides of the cover plates as seen by discolorations and distinct outlines of the material test samples.[6] This would increase the thickness in the center where the evidence of corrosion on the inside of the cover plates was the greatest.
3. Corrosion was as predicted but left an oxide that maintained the thickness. This one is unlikely since the cover plates were still shiny on the outside, the side in the flowing water stream. An oxide of the thickness predicted in Fig. 13 should leave a discoloration.

[5] It is conceivable that the corrosion is due to intermediate lifetime radiolysis products lasting long enough to skew the corrosion distribution to a sigmoid-like one that does not peak in the center. But this distribution would then show up in the Table 7 as a thinning in the center and at the downstream end (in the water flow sense). To be a viable model, the products would have to react before reaching Probe 40 in the next manifold section.

[6] Nitric acid may have formed in the humid air trapped inside the envelopes during welding.

4. The cover plate estimate includes an extrapolation of Fig. 3 to 1 mA average current. Possibly, the curve begins to roll over faster that the power 0.95, i.e., an increasing saturation with average current.
5. The corrosion profile is actually peaked, but the EIS predictions are too high, leaving the peaking undetectable.

Discussion

Modifications to corrosion rates derived solely on power density may be necessary because the operable corrosion mechanism may be responsive to differing radiation fields the APT plant, e.g., the fact that the neutron flux is higher in the APT production plant than in the LANSCE experiments that were used to derive Eq. 4 and Fig. 10.

Proposed explanations for the radiation-enhanced corrosion can be categorized by response/ recovery times. We know that the initial effects of the radiation (scattering, ionization, excitation, displacement damage, etc.) occur very rapidly. And we have seen a time constant (the order of 1 ms) in our data that motivated the transient modeling studies [2], but we do not know the type of radiation responsible for the time constant nor the explanation of the corrosion enhancement. The existence of a transient implies that the corrosion rate increases in some way to the beam pulse and then recovers, and we shall examine the time scales of the effects that are usually mentioned for explaining radiation effects in corrosion in order to look for transients.

1. Radiation can strongly influence reaction rates by breaking bonds that ordinarily have to wait for thermal energy, thus accelerating the kinetics of allowed reactions. In this capacity, any ionizing radiation will cause this effect to occur, and the power density would be a good predictor for the effect. In the Point Defect Model (PDM) of passive oxides [7], the reaction rate constants at the barrier layer interfaces enter into the film growth rates (corrosion). While the reaction rate constants would return to normal after the beam ceases, a persistence or relaxation back to steady state may occur in the vacancy concentrations set up within the barrier layer by the increased reaction rates.
2. Water radiolysis products are produced very rapidly, and all ionizing radiation contributes to these processes. Assuming that water is present on the solution side of the barrier layer, radiolysis radicals can dramatically increase the production and consumption of the cation and anion vacancies that transport metal and oxygen ions through the barrier layer. As with radiation effect 1, above, the reaction rates would return to normal after the beam ceases, but relaxation back to steady state may occur in the vacancy concentrations set up within the barrier layer by the increased reaction rates on the solution side of the barrier layer.
3. Electrical properties of the semiconducting barrier layer, such as conductivity, are affected by radiation, for example, by the creation of electron-hole pairs, and in this capacity any ionizing radiation will cause this effect to occur. The main point is that these carriers die off after the radiation goes off, with no obvious persistence effect. These carriers play a role, but do not appear to be rate limiting in the PDM.
4. Lillard and Daemen have seen that proton irradiation alters the dielectric properties of the passive oxide film in tungsten [8] which suggests changes in the oxygen transport properties through the oxide film and therefore changes in corrosion rate. In the PDM, the electron donors in the semiconducting barrier film are the defects themselves, the oxygen vacancies. Intense proton and neutron fluxes produce copious numbers of point defects, some of which

form vacancies that directly affect metal and oxygen ion transport. Short time scale relaxation of this structural damage is not known but conceivable.

5. Experimentally, we have seen that the recovery after the first beam exposure is not complete since the corrosion rate does not return to the pre-beam condition. We were able to look on the time scale it takes to make a measurement (20 minutes). Some "permanent" damage has apparently occurred, unlike the electronic changes that disappear after beam is off. Just as with the effect described in 4, this is suggestive of structural damage to the passive oxide layer, induced by nuclear scattering, i.e., neutron damage to semiconductor materials. This structural damage also changes the electrical properties of the passive oxide layers, determined to be highly doped semiconductors.[7] As for a relaxation effect, one is the corrosion itself that reconstitutes the layer. For a very thin barrier film, it is possible to "repair" it through corrosion on the time scale needed.

A related issue, the Probe 35-38 discrepancy, also bears discussion. The corrosion rate measured for Probe 38, Figs. 2 and 5, has 38% higher corrosion rate than that measured for Probe 35 even though the power density is the same. Dominated by the protons, the power density is the same because the probes are the same distance from the beam axis. The photon flux ratio of Probes 38 and 35 is in the right direction but only "accounts" for 5% out of the 38% discrepancy (Table 5). Neutron flux therefore is a better predictor than the gamma flux, "accounting" for 15% out of the 38% discrepancy (Table 5). The fourth described radiation effect, above, is the one to try here. As a matter of practicality, we propose to use the material damage parameter, displacements per atom (dpa) in the metal as a predictor for corrosion rate. The dpa accumulation rate, which includes the effects of neutrons and protons, might not be the operable radiation effect on corrosion, but it might well be proportional to the operable effect (e.g., defect density, oxygen vacancies). However, this most promising avenue is not anticipated to be fruitful in explaining the discrepancy because the material damage directly in the beam is dominated by the protons and is influenced only to a small extent by the neutrons because of the lower neutron flux relative to the proton flux at the locations of Probes 35 and 38.

Of the five radiation effects mentioned above, some are predicted well by power density alone and others are a consequence of nuclear scattering of protons and neutrons. For applications and/or locations where neutrons are prevalent, we recommend scaling up the predictions of Eqs. 3 & 4 by dpa accumulation rates. For the APT production plant with its higher neutron flux, this amounts to a factor of 2 increase in corrosion rate.

Conclusions

Correlations between corrosion rate and radiation intensity computed by MCNPX have been found for 316L SS and permit extrapolation to the raster beam conditions in the APT production plant. The formula makes use of the observation that the corrosion efficiency drops as the instantaneous radiation intensity increases, thus reducing corrosion projections in the rastered beam of APT. Using total power density as the measure of radiation intensity, a corrosion rate of 20 μm/y is projected for 316L SS. As a result of the corrosion efficiency, the rastered APT beam has a factor of 5 lower corrosion rate than would be obtained for an expanded dc beam that was once considered for APT targeting.

The discovery of a time constant is significant, as is the finding of a saturation effect at these high power densities. The time constant found, in one interpretation, is the order of the widths of

the beam pulses (600 μs) and suggests both theoretical consideration and further pulsed beam studies.

References

[1] R.S. Lillard, F. Gac, M. Paciotti, P. Ferguson, G. Willcutt, G. Chandler, and L.L. Daemen, "The Effects of High Energy Proton Radiation on the Corrosion of Materials", *Effects of Radiation on Materials:20th International Symposium, ASTM STP 1405*, S.T.Rosinski, M.L. Grossbeck, T.R. Allen, and A.S. Kumar, Eds., American Society for Testing and Materials, West Conshonhocken, PA, 2000.

[2] Lillard and Paciotti, "A Model for Analyzing Corrosion Data from Pulsed Proton Beam Irradiation Experiments", Accepted for publication in JOM.

[3] R.S. Lillard, D.l. Pile and D.P. Butt, "The Corrosion of Materials in Water Irradiated by 800 MeV Protons," Journal of Nuclear Materials 278 (2000) 277-289.

[4] "Corrosion Testing in Support of the Accelerator Production of Tritium Program (U)," G.T. Chandler, K.A. Dunn, M.R. Louthan Jr., J.I. Mickalonis, F.D. Gac, S.A. Maloy, M.A. Paciotti, W.F. Sommer, Jr., and G.J. Willcutt, Jr., *Proceedings of the 2001 NACE International Annual Conference CORROSION 2001*

[5] Cappiello, M. and Pitcher, E., "Design and Operation of the APT Target/Blanket", Materials Characterization 43:73-82 (1999).

[6] Maloy, S. A., James, M. R., Willcutt, G. J., Sommer, W. F., Johnson, W.R., Louthan, M. R., Hamilton, M. L., Garner, F. A., "The Effect of High Energy Protons and Neutrons on the Tensile Properties of Materials Selected for the Target and Blanket Components in the Accelerator Production of Tritium Project," *Effects of Radiation on Materials: 20th International Symposium, ASTM STP 1405*, S. T. Rosinski, M. L. Grossbeck, T. R. Allen, and A. S. Kumar, Eds., American Society for Testing and Materials, West Conshohocken, PA, 2002.

[7] Macdonald, DD, "Passivity—the key to our metals-based civilization", Pure Appl. Chem., Vol. **71**, No. 6, pp. 951-978, 1999.

[8] Lillard, R.S., and Daemen, L.L., "The Influence of Radiation on the Passivity of Tungsten", Electrochimica acta, **147**, (June 2002).

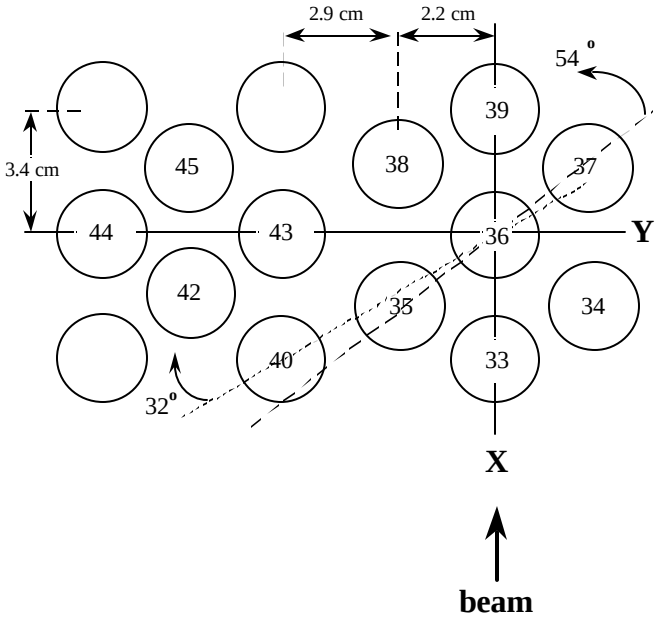

Figure 1 A schematic of the tube array irradiated at the LANSCE A6 target station. Three of these tubes contained Alloy 718 corrosion samples, Tube 33, Tube 39, and Tube 45. Tubes 36, 35, 38, 40 contain 316L probes. Tube 34 contains an Alloy 625 probe, and Tube 37 contains an Alloy C276 probe.

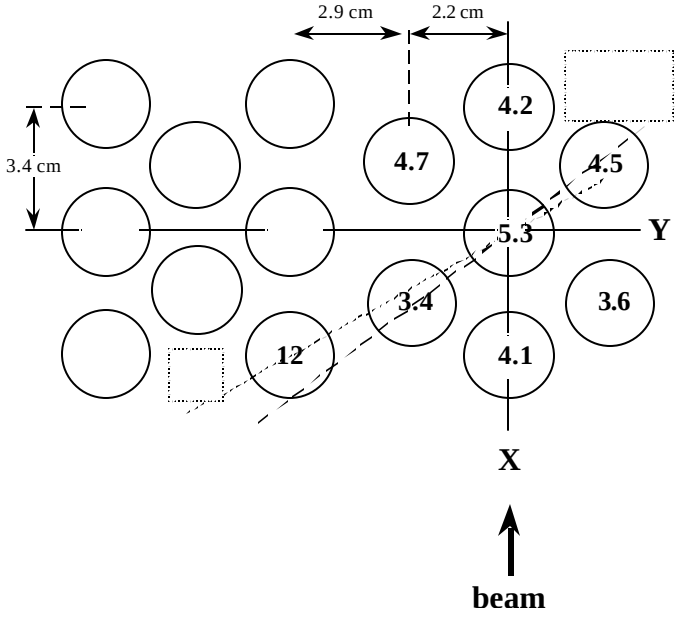

Figure 2 The same tube array of Fig. 1 where corrosion rates in mm/y are displayed inside the circles representing the water tubes. The point is that all of these corrosion resistant materials in proximity to the beam have similar corrosion rates. Beam current is 340 mA.

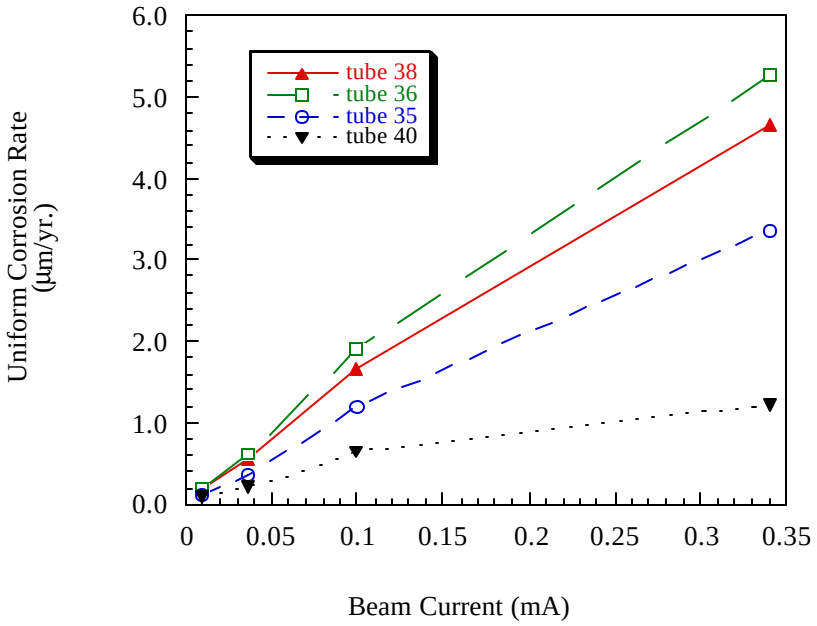

Figure 3 Corrosion rate as a function of average beam current for 316L SS probes. [1] Refer to Fig. 1 for tube locations. The peak current is the same for all data points.

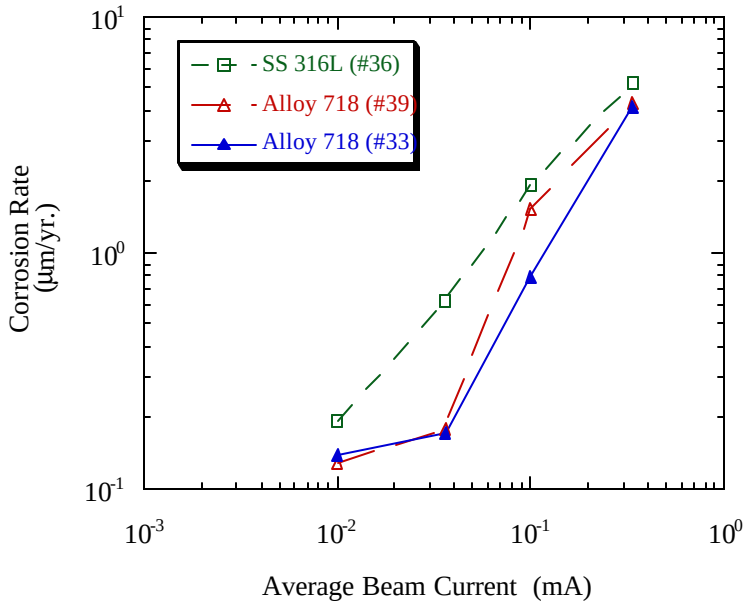

Figure 4 Corrosion rate as a function of average beam current. The peak current is the same for all data points.

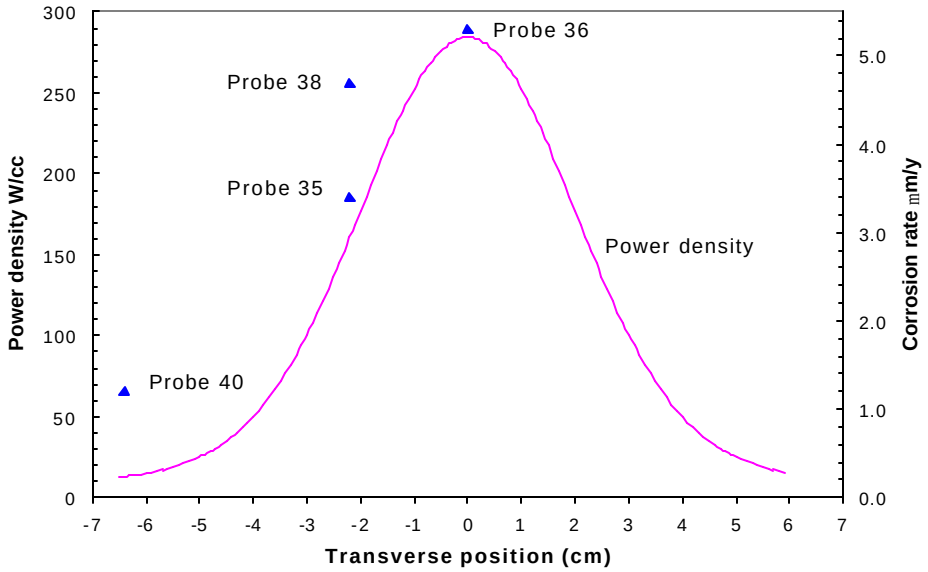

Figure 5 Comparison of the power density profile (solid curve) and corrosion rates (points) for 316L SS probes. The corrosion rates do not fall off as rapidly as the power profile. Probes 35 and 38 differ substantially. The horizontal position of the vertically mounted probes is plotted.

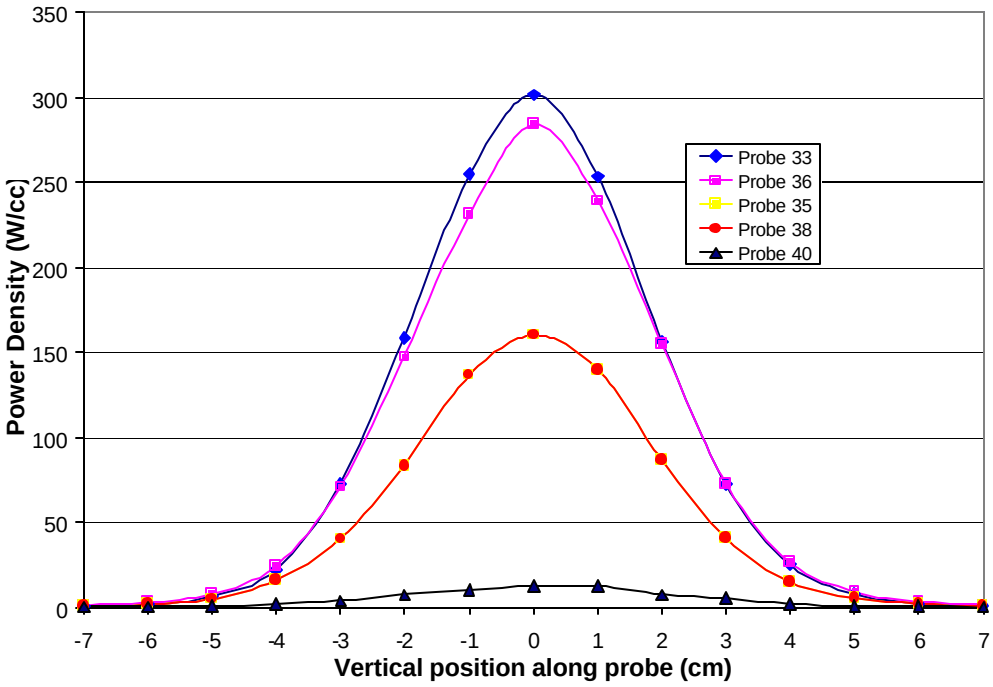

Figure 6 Time-averaged power density as a function of the vertical position (along the length of the probe). Zero cm is the center of the proton beam. Probe 33 is Alloy 718 and the others are 316L SS. Probes 35 and 38 are transversely equidistant from the center of the beam and the power curves are nearly identical.

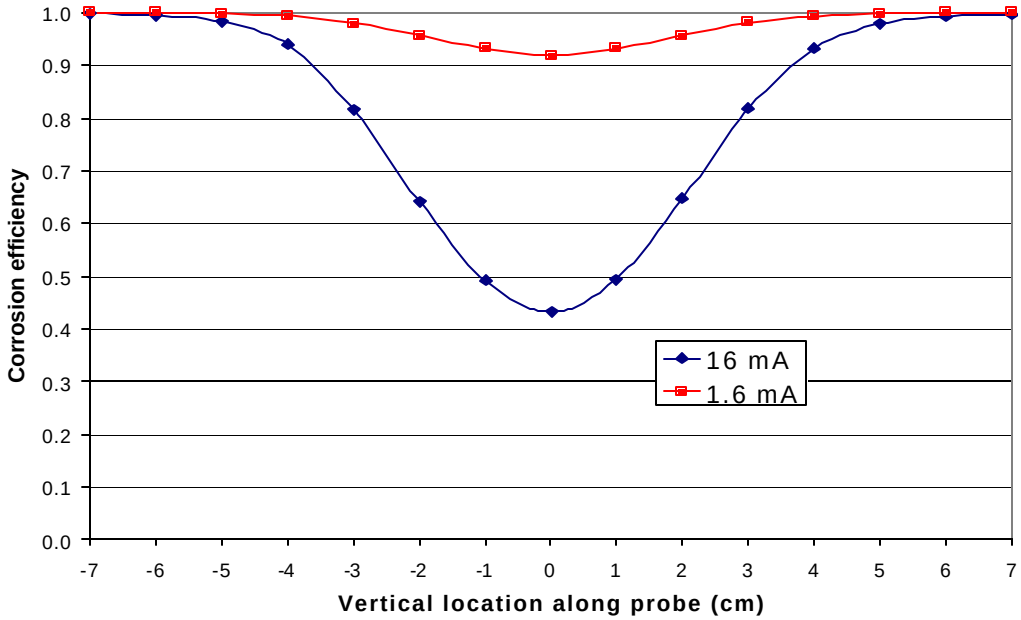

Figure 7 Corrosion efficiency variation along the length of Probe 33 for two instantaneous proton beam currents.

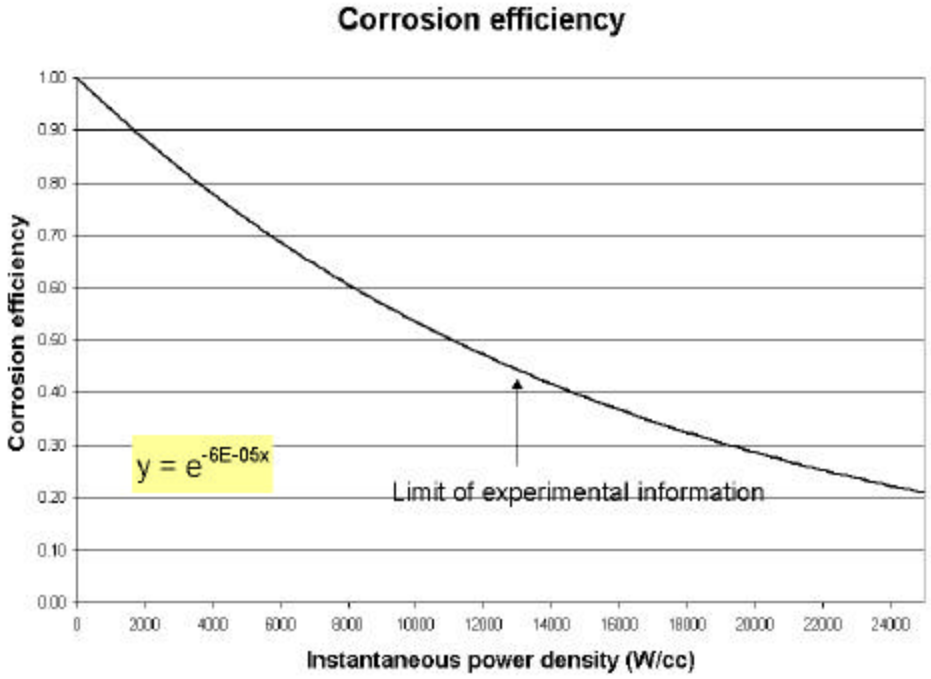

Figure 8 – *Corrosion efficiency as function of instantaneous power density. No experimental information is available beyond an instantaneous power density of 13000 W/cc. Data points do not appear because the contribution from each probe is a range of Instantaneous Power Density, with a shape like Fig. 6.*

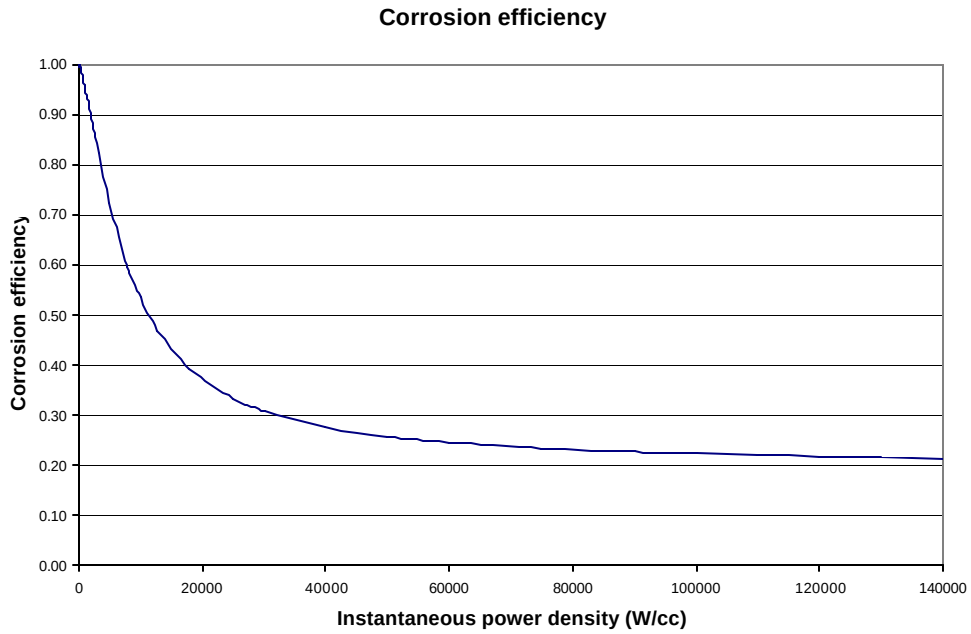

Figure 9 *Extrapolated Corrosion efficiency as function of instantaneous power density. This function tracks Figure 8 to the limit of the experimental information.*

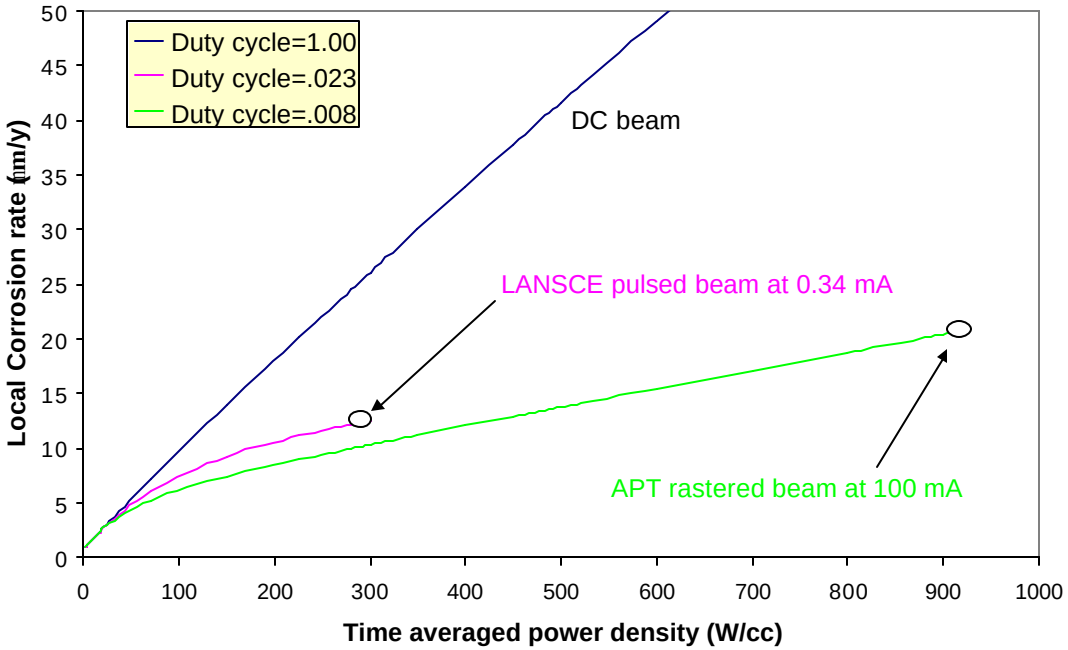

Figure 10 *Corrosion rate as a function of average power density for different beam duty cycles. The rollover of corrosion rate is due to the corrosion efficiency.*

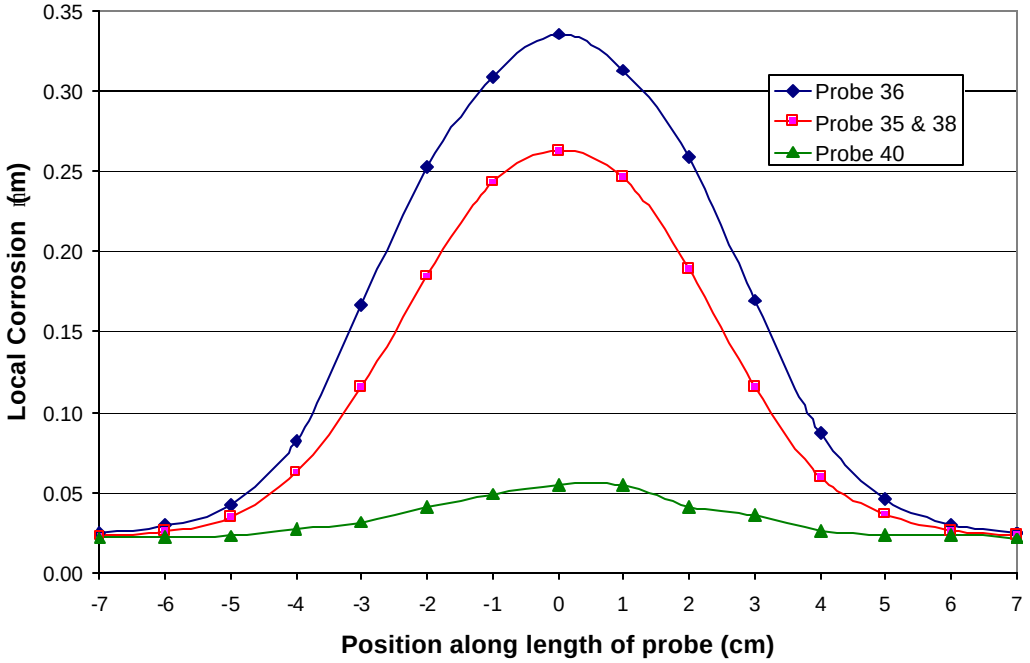

Figure 11 – *Corrosion profile for Probes 36,35,38, and 40 as predicted by the corrosion formula. 340 mA is impinging on the corrosion experiment with no other material upstream. 10 days irradiation time.*

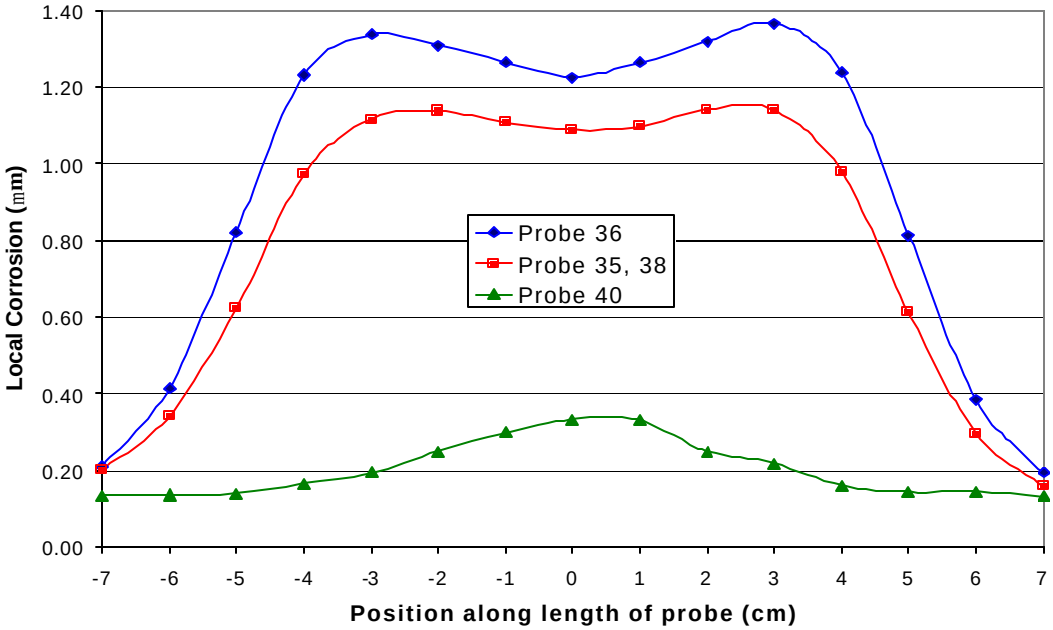

Figure 12 *Corrosion profile for Probes 36,35,38, and 40 as predicted by the corrosion formula. 950 mA is impinging on the full array of APT experiments, with the corrosion one being last. The central dip is due to the protons interacting with the horizontal tungsten elements upstream of the vertically oriented corrosion probes. 2 months irradiation time.*

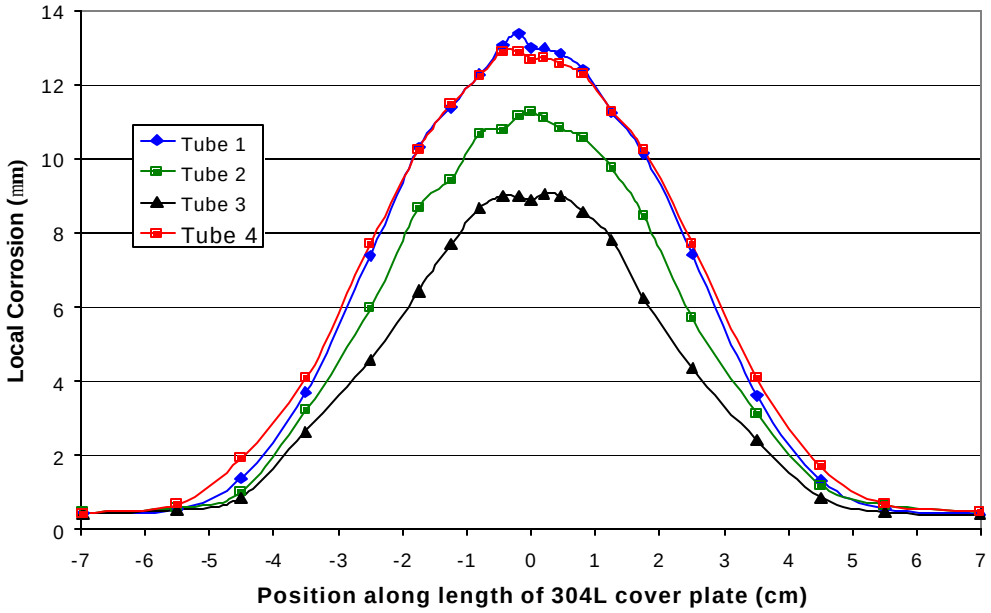

Figure 13 Predicted corrosion of the 304L cover plates (envelopes) that kept the cooling water from contacting the APT materials irradiation samples. 6 months irradiation time.